Vortex Nano-Oscillators Based on Magnetic Tunnel Junctions for Neuromorphic Applications

João Miguel Soares da Silva
Mestrado em Engenharia Física
Departamento de Física e Astronomia
2022

Orientador
Prof. Dr. João Oliveira Ventura, Faculdade de Ciências

Coorientador
Dr. Ricardo Ferreira, International Iberian Nanotechnology Laboratory

U.PORTO

FACULDADE DE CIÊNCIAS
UNIVERSIDADE DO PORTO

Todas as correções determinadas pelo júri, e só essas, foram efetuadas.

O Presidente do Júri,

Porto, _____/_____/_____

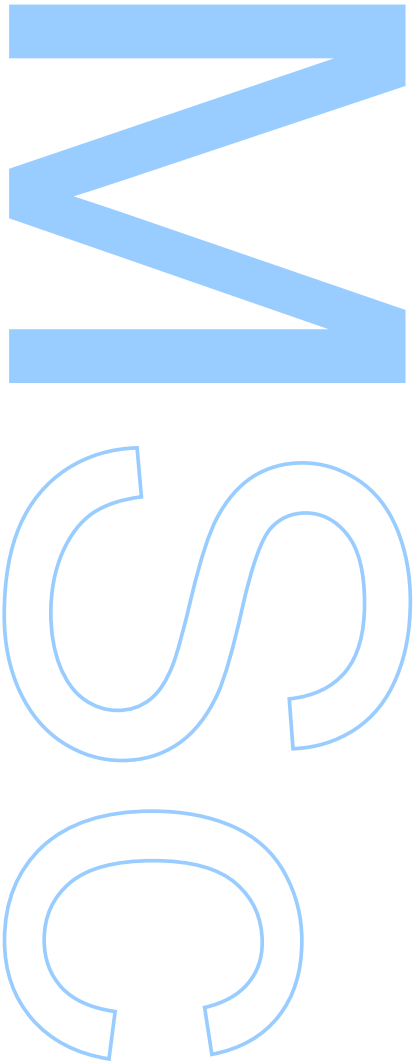

UNIVERSIDADE DO PORTO

MASTERS THESIS

Vortex Nano-Oscillators Based on Magnetic Tunnel Junctions for Neuromorphic Applications

Author:
João Miguel SOARES DA SILVA

Supervisor:
João OLIVEIRA VENTURA

A thesis submitted in fulfilment of the requirements
for the degree of MSc. Engineering Physics

at the

Faculdade de Ciências da Universidade do Porto
Departamento de Física e Astronomia

November 28, 2022

Declaração de Honra

Eu, João Miguel Soares da Silva, inscrito no Mestrado em Engenharia Física da Faculdade de Ciências da Universidade do Porto declaro, nos termos do disposto na alínea a) do artigo 14.º do Código Ético de Conduta Académica da U.Porto, que o conteúdo da presente dissertação reflete as perspetivas, o trabalho de investigação e as minhas interpretações no momento da sua entrega.

Ao entregar esta dissertação, declaro, ainda, que a mesma é resultado do meu próprio trabalho de investigação e contém contributos que não foram utilizados previamente noutros trabalhos apresentados a esta ou outra instituição.

Mais declaro que todas as referências a outros autores respeitam escrupulosamente as regras da atribuição, encontrando-se devidamente citadas no corpo do texto e identificadas na secção de referências bibliográficas. Não são divulgados na presente dissertação quaisquer conteúdos cuja reprodução esteja vedada por direitos de autor.

Tenho consciência de que a prática de plágio e auto-plágio constitui um ilícito académico.

João Miguel Soares da Silva
Porto, 28 de novembro de 2022

Acknowledgements

I'd first like to thank my supervisor João Ventura for all of his time and patience in my begginer problems, as well as Dr. Ricardo Ferreira and Alex Jenkins, who allowed me the opportunity to work with the International Iberian Nanotechnology Laboratory (INL) for my master thesis. I equally need to praise Luana Benetti and Alejandro Schulman for showing me around the clean room and fabrication techniques during my stay at INL. I'd also like to thank Maria Grácio, for the help we gave each other on the begining of both our dissertations, and Catarina Dias, the person with whom I started researching in past internships, who was always willing to explain me the obvious.

I'd like to express my deep gratitude to all of my friends for keeping me sane during this five difficult years. Specially, I want to express my gratitude to António Correia, Bernardo Campilho, João Araújo and Rodrigo Silva, who've been with me since most of my university life, as well as my friends who I've known even since before the start of this journey. They are Daniel Plácido, João Neves, João Nogueira and Jorge Lopes, without whom I couldn't have completed this course.

Most of all, I'd like to thank my parents, my brother and all of my family, for allowing me to do this in the first place.

UNIVERSIDADE DO PORTO

Abstract

Faculdade de Ciências da Universidade do Porto
Departamento de Física e Astronomia

MSc. Engineering Physics

Vortex Nano-Oscillators Based on Magnetic Tunnel Junctions for Neuromorphic Applications

by João Miguel SOARES DA SILVA

Until recently, spintronic research relied solely on external magnetic fields to manipulate the spin of the electron. However, electrical currents were also recently shown to be able to tune the magnetic behavior of nanoscale magnetic tunnel junctions (MTJs). In collaboration with the Iberian Institute of Nanotechnology (INL) in Braga, in this work we studied MTJs with strongly pinned magnetic vortices in the free layer.

In this thesis, at INL, MTJs based on micro and nanopillars with an insulating MgO layer were fabricated with different properties, in particular, both MTJs with $NiFe$ and $CoFeSiB$ layers were fabricated and will be compared. We shall then study how these devices change when different magnetic fields, voltages and temperatures are applied.

We have verified that the system can jump into different values while in its vortex state, when a high enough voltage is applied. Besides that, we were also able to obtain an emergence of hysteretic behavior at low temperatures. Such behavior can have potential applications in neuromorphic computation, including reservoir computing.

UNIVERSIDADE DO PORTO

Resumo

Faculdade de Ciências da Universidade do Porto
Departamento de Física e Astronomia

Mestrado em Engenharia Física

Nano-Osciladores com Vórtices Baseados em Junções Magnéticas de Efeito Túnel Para Aplicações Neuromórficas

por João Miguel SOARES DA SILVA

Até recentemente, pesquisa em eletrónica de spin dependia apenas de campos magnéticos externos para manipular o spin do eletrão. No entanto, correntes elétricas também mostraram recentemente ser capazes de ajustar o comportamento magnético de junções de efeito túnel (MTJs) em nanoescala. Em colaboração com o Instituto Ibérico de Nanotecnologia (INL) em Braga, neste trabalho estudamos MTJs com vórtices magnéticos fortemente presos na camada livre.

Nesta tese, no INL, MTJs baseados em micro e nanopilares com uma camada isoladora de MgO foram fabricados com diferentes propriedades, em particular, foram fabricados MTJs com camadas de $NiFe$ e $CoFeSiB$, que serão comparadas. Estudaremos então como esses dispositivos mudam quando diferentes campos magnéticos, tensões e temperaturas são aplicadas.

Verificamos que o sistema pode saltar para diferentes valores enquanto em seu estado de vórtice, quando uma tensão suficientemente alta é aplicada. Para além disso, também conseguimos obter um surgimento de comportamento histerético para baixas temperaturas. Tal comportamento pode ter potenciais aplicações em computação neuromórfica, incluindo computação de reservatório.

Contents

List of Figures

Glossary

AFM	Antiferromagnetic
ANN	Artificial Neural Network
DOS	Density of States
FM	Ferromagnetic
GMR	Giant Magnetoresistance
LIF	Leaky Integrate and Fire
LLGS	Landau–Lifshitz–Gilbert–Slonczewski
MTJ	Magnetic Tunnel Junction
TMR	Tunnel Magnetoresistance

Chapter 1

Introduction

We shall begin this first chapter with an overview of magnetism, spintronics and the effect of tunnel magnetoresistance (TMR) that can be seen in magnetic tunnel junctions (MTJs). Finally, we will present the motivation for this work and discuss how this thesis is organized.

1.1 Basic Concepts in Magnetism

Since the discovery of magnetism, in the ancient period, the interest in the subject has grown. As we gained knowledge of how the mechanism works, we were able to manipulate it and create several applications in very different fields, such as electronics, medicine, and so on. Magnetism has had a vast journey, from the discovery of magnetite, the development of the compass, revolutions in the field by Maxwell, Faraday and more, and even its presence in the military during both world wars, magnetism has seen many uses and applications.

Thanks to the development of quantum mechanics, statistical physics and the study of nanotechnologies, a new era of magnetism has begun: the era of spintronics [1]. Physicists Fert and Grünberg are two big names associated with this new era we find ourselves in. However, before diving into this subject, we should review some basic concepts used in magnetism.

Magnetic materials can be classified in different ways, according to the behaviour of their magnetic moments and how they respond to an external magnetic field [2]. In a magnetic material, we may observe (figure 1.1):

- diamagnetism - effect that makes magnetic moment align in opposition to the external magnetic field, returning to a null net magnetic moment as soon as the magnetic field is removed;
- paramagnetism - similar to diamagnetism; however, magnetic moments are aligned with the external magnetic field (not opposing it);
- ferromagnetism - alignment of all magnetic moments of the atoms in the same direction, following a hysteresis loop, such that a net magnetization remains even after the magnetic field is removed;
- antiferromagnetism - magnetic moments are arranged in an antiparallel configuration such that the magnetic moments cancel out;
- ferrimagnetism - Arrangement of magnetic moments in an antiparallel configuration such that the magnetic moments do not completely cancel out (since different ions have a different magnitude in their magnetic moments) and a net magnetization remains.

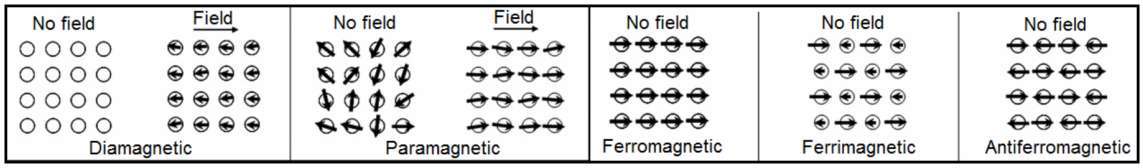

FIGURE 1.1: Magnetic dipoles and their behavior when a magnetic field is applied (credits: [3] U. Jeong, *et al.*, 2007).

In figure 1.2, we can see the behaviour for a ferromagnetic material, showing the hysteresis loop mentioned above. However, we should note that this only happens along the "easy axis" (the direction in which the magnetic dipoles tend to align). This is because, since the dipoles are stable in that direction, it's difficult to change their orientation, and they will only flip when a certain magnetic field H_c is applied. If the field is applied in a 90° angle, in what is called the "hard axis", the magnetization gradually changes until it reaches the saturation magnetization M_s.

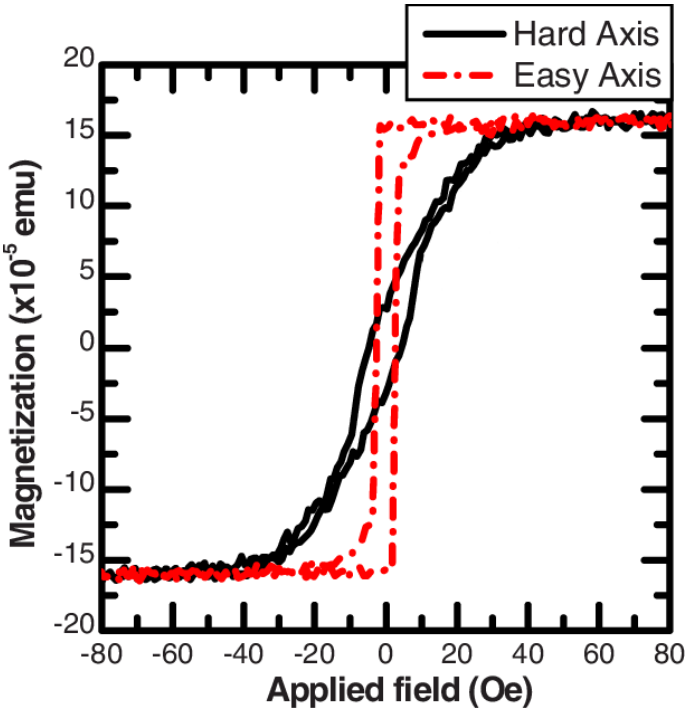

FIGURE 1.2: Magnetization for the easy axis (in red) and the hard axis (in black) as a function of the applied magnetic field (credits: [4] Daniel Kirk, *et al.*, 2009).

1.2 Spintronics Overview

Spintronics [1] refers to a new way of constructing and thinking about magnetic devices. While conventional electronics ignores the spin of the electron, spin electronics makes use of this property in order to create new materials and devices.

In order to dive deep in the field of spintronics, the first step is to talk about magnetoresistance. This effect refers to the ability of some materials to change their electrical resistance when subjected to an external magnetic field. In the simplest case, in giant magnetoresistance (GMR), the principle is born from the fact that, when an electron is travelling through a magnetized lattice, it experiences a lower resistance if the orientation of the magnetization matches that of the electron's spin.

With this is mind, we can create a device that changes its resistance depending on the applied external magnetic field. For instance, let's consider the simple case of a spin valve [5, 6]. This device starts with an antiferromagnetic (AFM) layer, followed by a ferromagnetic (FM) one. This FM layer is considered to be fixed because, due to the interaction (exchange bias) with the AFM material, it needs a large external magnetic field to change its magnetization. Above this layer, a non-magnetic metal is deposited (called a "spacer")

and then another FM layer above that (this one considered to be "free", since we can easily change its magnetization).

Therefore, when applying a magnetic field, only the free layer will change its magnetization (unless a high enough field is applied to change the fixed layer), which changes the resistance of the device. This can be explained with the help of figure 1.3, where we think about current as traveling through two independent channels, one of them with spin-up electrons and the other with spin-down. Since the resistance of each electron depends on its spin and the magnetization of the environment, if both FM layers are magnetized in the same orientation (parallel configuration), the total resistance will be lower than in the situation where the layers have different orientation (antiparallel configuration). In fact, the bigger the angle of the magnetization between the two layers, the higher the resistance will be.

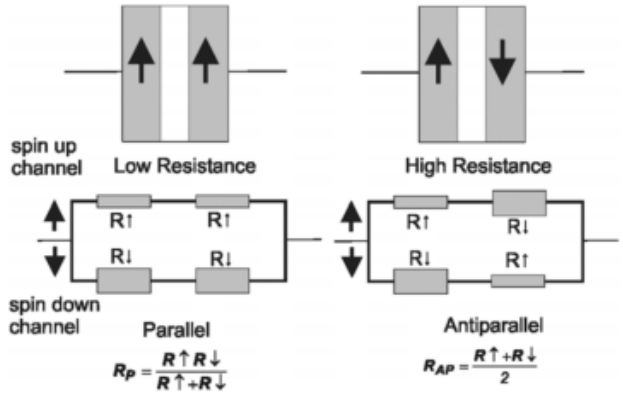

FIGURE 1.3: Schematic figure of GMR in a spin valve with 2 ferromagnetic layers (source: [7] Sarah M Thompson, 2008). On the left we see the parallel configuration, with lower resistance, while on the right we see the antiparallel configuration, with higher resistance.

One of the ways we can obtain a value for the magnetoresistance is by:

$$MR = \frac{R_{max} - R_{min}}{R_{min}}(\%). \tag{1.1}$$

1.3 Tunnel Magnetoresistance

When we talk about magnetic tunnel junctions (MTJs), the physics changes [8, 9]. Instead of a metal being used as a spacer, an insulator with a thickness of 1 nm or less is used. Although not conductive, this layer is thin enough to allow electrons to pass by quantum tunneling. This being the case, it means the electrical terminals must be in different FM

layers to force tunneling to happen. It also implies that any defect in the spacer layer is dangerous, since it might favor electrons to take a particular path through that region.

The physics behind tunnel magnetoresistance (TMR) can be explained by using density of states (DoS), as we see in figure 1.4, but the basic operating principle is the same as spin valves and we can still use equation 1.1 to obtain the TMR of the device. The conductance $G = 1/R$ can be expressed as a function of the angle θ between the spin and the lattice's magnetization [10] according to:

$$G(\theta) = \frac{1}{2}(G_P + G_{AP}) + \frac{1}{2}(G_P - G_{AP}) \cdot \cos\theta, \tag{1.2}$$

where G_P is the conductance in the parallel configuration (highest value) and G_{AP} the conductance in the anti-parallel configuration (lowest value).

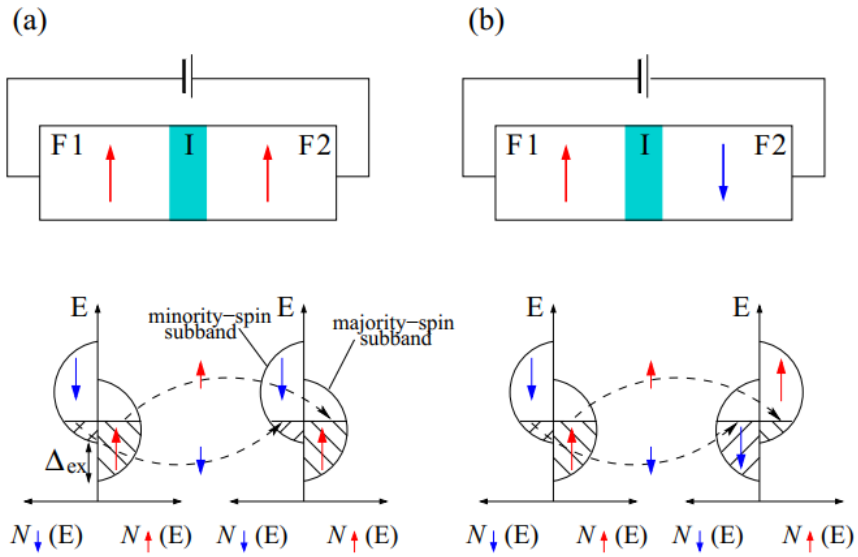

FIGURE 1.4: Schematic showing the electron tunneling in a magnetic tunnel junction, with two ferromagnetic layers and an insulating barrier in its (a) parallel and (b) antiparallel orientations. It's also shown the corresponding spin-resolved density of the d states in the ferromagnets, with dashed lines representing the spin-conserved tunneling (credits: [11] Igor Žutić, *et al.*, 2004).

1.4 Julliere's Model

The explanation of the physics that reigns over TMR was first attempted by Julliere [12]. In it, he made two assumptions. The first assumption is that the electrons travel without spin flip, which means that we consider a separation of the majority and minority spin between two channels [13, 14]. The second assumption says that the current of a certain

spin is proportional to the product of the effective DoS durring tunneling. We can derive that [13, 15, 16]:

$$I_P = I_\uparrow + I_\downarrow \propto N_1^\uparrow N_2^\uparrow + N_1^\downarrow N_2^\downarrow, \tag{1.3}$$

$$I_{AP} = I_\uparrow + I_\downarrow \propto N_1^\uparrow N_2^\downarrow + N_1^\downarrow N_2^\uparrow, \tag{1.4}$$

where I_P (I_{AP}) is the current in the parallel (antiparallel) configuration, N_i (with $i = 1, 2$) refers to the density of states (DoS) at the Fermi level for the first ($i = 1$) and second ($i = 2$) ferromagnetic layer and for the the majority-spin ($N_i^\uparrow$) and minority-spin ($N_i^\downarrow$) electrons.

With the help of experimental data from Tedrow *et al.*, in the 1970s [16], who used superconducting layers as detectors to measure spin polarization tunneling (SPT), Julliere's model also says that the spin polarization of each ferromagnetic layer P_i is given by:

$$P_i = \frac{N_i^\uparrow - N_i^\downarrow}{N_i^\uparrow + N_i^\downarrow}, \tag{1.5}$$

Taking the preceding equations 1.3-1.5 into consideration, we arrive to the final equation for the TMR of a device, given by:

$$TMR = \frac{2P_1P_2}{1 - P_1P_2}. \tag{1.6}$$

1.5 Motivation

In this thesis, we will explore the topic of spintronics and how new applications can be derived from spin dependent transport. Specifically, we want to study how granularity-induced vortices can influence the spintronic devices and make new properties emerge.

Until recently, research in spintronics primarily depended on external magnetic fields to manipulate the spin of the electrons. However, electrical currents were also recently shown to be able to tailor the magnetic behavior of nanoscale magnetic tunnel junctions [17]. Novel applications, including chip-to-chip wireless communication or neuromorphic electronics become possible as a result.

In a collaboration with the Iberian Institute of Nanotechnology (INL) in Braga, in this dissertation we aim to develop and study magnetic tunnel junctions with novel magnetic textures. In particular, by controlling the granularity of the devices we aim to obtain strongly pinned magnetic vortices in the free layer and verify if such behavior can have

potential applications in neuromorphic computation [18]. Likewise, we intend to analyse different types of compositions to find out if new properties emerge from it.

1.6 Organization of This Thesis

After this brief introduction of spintronics, as well as the motivation for this thesis, in chapter 2, we shall present a description of how these magnetic tunnel junctions work in more detail, elaborating in more concrete topics that are going to help us with this particular work. For instance, we shall examine how the atomic structure of the insulating layer influences its properties, how temperature and voltage change the MTJ's behaviour, as well as the effect that vortices have on it.

Chapter 3 includes the experimental techniques used in this work. This refers to some basic notes on the fabrication method of the MTJs, used at INL, and an elaborated description of the characterization techniques that we are going to use to analyse the samples and determine its properties.

In chapters 4 and 5 we'll analyse the data obtained from the measurements described in chapter 3. We shall make a description of how the properties of our MTJ's changed with the applied magnetic field, voltage bias and temperature.

Finally, in chapter 6 we present a summary of the most important results and finish with this thesis conclusion, including some future work that can still be done in this area.

Chapter 2

Physics Behind MTJs and Nano-Oscillators

2.1 Difference between amorphous and crystalline barriers

Bloch's theorem says that the eigenstates ψ of an electron in a periodic potential are given by a plane wave multiplied by the Bloch function $u_k(r)$ with the same period as the lattice [2], which means they have the form:

$$\psi_k(r) = u_k(r) \exp(ik \cdot r). \tag{2.1}$$

The tunneling probability of an electron depends on the rate of decay of its wave function in the barrier of the MTJ, which depends on the symmetry of the atomic orbitals.

In an amorphous material, the structure of the insulating barrier lacks crystallographic symmetry and the tunneling probability is independent of the Bloch state symmetry of the electron [8]; therefore, all undergo the same decay rate. In figure 2.1(a), this is shown with the tunneling through an amorphous $Al - O$ barrier. We refer to this effect as incoherent tunneling.

In crystalline barriers, we have coherent tunneling with symmetry dependent decay, as we see represented in figure 2.1(b). With this method, we're able to obtain the highest TMR values. Nagamine et al. [20] obtained TMR values above 50% from MTJs with a crystalline MgO barrier and a RA product below $1\Omega\mu m^2$.

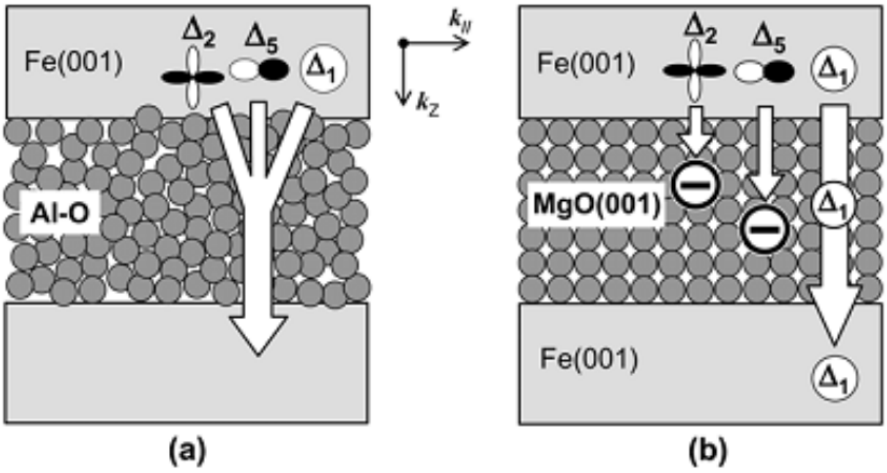

FIGURE 2.1: Schematics of electron tunnelling through (a) an amorphous $Al-O$ barrier and (b) a crystalline $MgO(001)$ barrier (credits: [19] S. Yuasa and D. D. Djayaprawira, 2007).

2.2 Temperature and Bias Voltage Dependence of the TMR

2.2.1 Bias Voltage Dependence

Studying how the tunnel magnetoresistance changes with the applied voltage is one of the factors we will want to examine. Analysing this dependence (figure 2.2), we see a symmetrical behaviour around $V = 0$, with $TMR(0) = TMR_{max}$ and where the TMR value decreases with the increase of the applied voltage.

A good analysis of this dependence is crucial for many applications, for it gives us the knowledge of how much voltage the device can take, how its behaviour changes and how stable it is. One of the main points we normally look at is the voltage $V_{1/2}$ for which the resulting TMR is half of the one where no bias is applied, i.e. the voltage that satisfies:

$$TMR(V_{1/2}) = \frac{TMR(0)}{2}. \tag{2.2}$$

A physical explanation for this effect is not yet clear; however, some studies have already been performed to try to correlate this phenomenon with magnon excitations or changes of the electronic band structure of the FM electrodes [8, 22, 23].

2.2.2 Temperature Dependence

We will also study how our system changes with different temperatures and for that we must realize that the magnitude of the TMR is temperature dependent, decreasing as temperature increases. There are many possible explanations for this behaviour [9]. It can

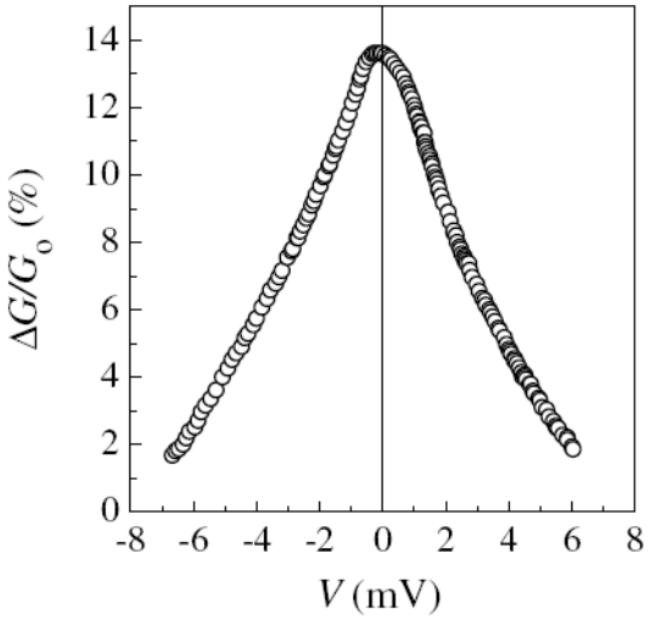

FIGURE 2.2: The first demonstration of the TMR effect in a $Fe/Ge/Co$ junction, measured at 4.2 K, where ΔG is the difference between the two conductance values corresponding to P and AP configurations of the two FM electrodes (credits: [21] Tsymbal, *et al.*, 2003).

be related to thermally excited magnons (high temperature electrons lose their excessive energy by the release of magnons which do not preserve electron spin, decreasing polarization), magnetic impurities, defects, temperature variation of electronic structure, and so on. Quantitatively [24], we have that the polarization P is related to the temperature T by:

$$P \propto \left(1 - \alpha T^{3/2}\right), \tag{2.3}$$

where α is a material-dependent constant.

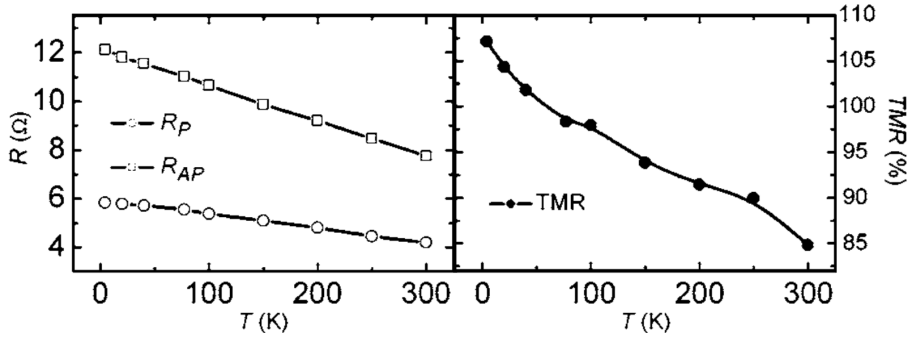

FIGURE 2.3: The resistance of the parallel (R_P) and anti-parallel (R_{AP}) configurations (on the left) and the TMR (on the right) as a function of temperature for a $CoFeB/AlO_x/CoFeB$-based MTJ (credits: [25] H. X. Wei, *et al.*, 2007).

Figure 2.3 shows the TMR behaviour for an MTJ with an AlO_x barrier and we can see that the total TMR decrease results mainly from the decrease of R_{AP}, while the R_P value does not decrease as much.

2.3 Vortices

The free layer starts with several magnetic domains, pointing in different directions. Applying a magnetic field, we first have the growth of domain walls and then rotation of the magnetic dipoles. The way we made them, the magnetic domains (the dipoles) directions are organized in a vortex with a center we will call the "vortex core". To be able to create these vortices, some conditions must be met, primarily, the L/R ratio must be carefully chosen [26], where R is the radius of the FM layer and L is its thickness.

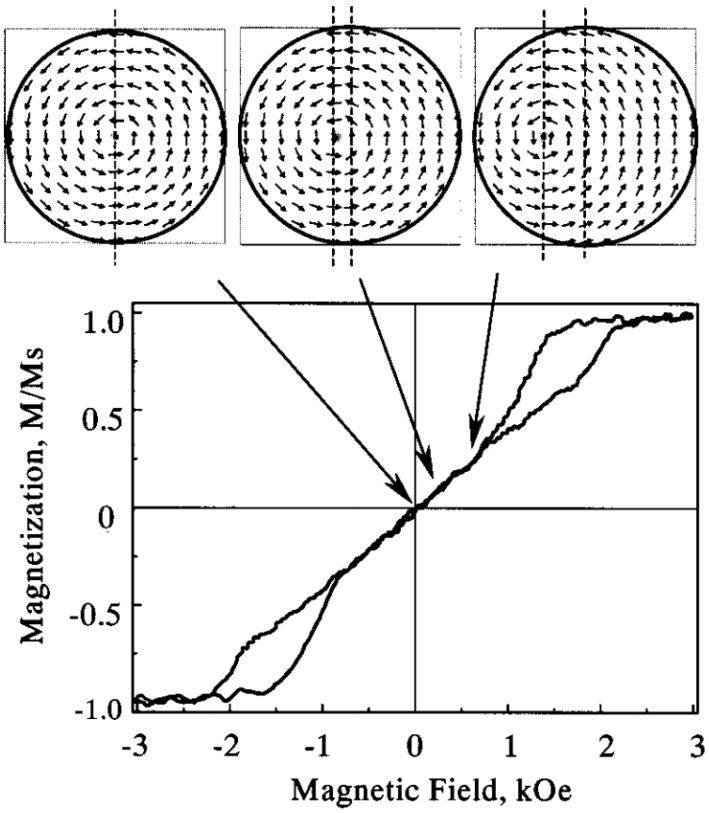

FIGURE 2.4: Normalized magnetization measurement of a magnetic vortex, with a schematic of the vortex behaviour (credits: [27] K. Y. Guslienko, *et al.*, 2001).

We can see that this changes the magnetization of the layer, since a core in the center will lead to null magnetization, but moving it to the side makes it so that a certain orientation wins over the other. When a magnetic field passes through the layer, we can think of it as the core moving around, as we see represented in figure 2.4.

These devices make use of these magnetization dynamics to form RF electrical signals. By controlling the current, we are able to control many parts of this system, e.g. the stochatic transition between the so called G-state and C-state [28, 29], but while in the vortex state, much more noise can be expected [30], since the core might get pinned in the defects present in the free layer. However, in this thesis, we won't explore radio frequency nor any of these dynamics, but understanding how we can manipulate the system with current is still useful.

In figure 2.5, we can see a summary of these behaviours of the vortex state, thanks to some measurements and simulations done at INL.

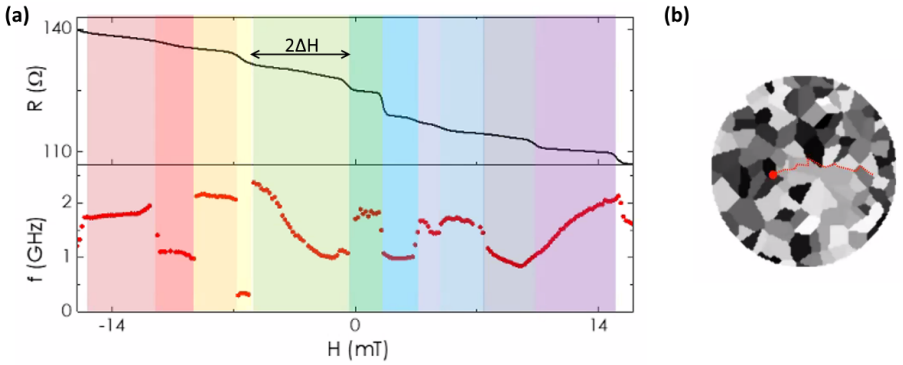

FIGURE 2.5: Expected behaviour of the samples, as measured at INL. In the left, we have (a) the behaviour of the resistance and frequency with the applied field, where we consider each interval between jumps (the width of each colored strip) as $2\Delta H$. In the right, we see (b) the black and white color plot of the grains (as simulated by micromagnetic simulations), with the red dot being the position of the vortex core.

When it comes to analysing these vortices in a quantitative manner, T. Y. Chen, *et al.* [31], in 2012, developed a way by calculating the energy of the pinning site, which, assuming a parabolic potential $W(r) = \frac{1}{2}k_u r^2$, is given by:

$$E_{pin} = \frac{1}{2}k_u r^2(\Delta H), \tag{2.4}$$

where $2\Delta H$ is the interval between two consecutive jumps (as seen in figure 2.5), $r(H) = \chi_0 RH/(M_s\xi)$ is the distance between the core and the disk center, H is the applied magnetic field, $k_u = M_s^2\xi^2 L\pi/\chi_0$ is the unpinned stiffness, M_s is the saturation magnetization, $\xi = 2/3$ is a model-dependent constant, $\chi_0 = R/10L$ is the vortex susceptibility, R is the radius of the disk and L is its thickness. Therefore, a given MTJ can be characterized by its E_{pin} values. For an easier calculation, we can directly use:

$$E_{pin} = \frac{\pi}{20}R^3 \cdot \Delta H^2. \tag{2.5}$$

2.4 Spin Transfer Torque and Nano-Oscillators

Let's consider a magnetic tunnel junction with a current travelling from the fixed layer to the free layer. When an electron travels through a magnetized lattice, it will tend to align with it and, by the conservation of angular momentum, the lattice's magnetization must slightly shift. This won't have much effect on the fixed layer; however, in the free layer, as electrons travel by, the exerted torque will make the layer inevitably align with the electrons arriving from the fixed layer, resulting in a parallel configuration.

If the current is going in the opposite direction, those opposing the magnetization of the fixed layer will travel back (due to the low density of states for that spin in the fixed layer), rotation the free layer to an anti-parallel configuration. Therefore, the direction of the current can be used to change the magnetization of the free layer, as seen in figure 2.6(a).

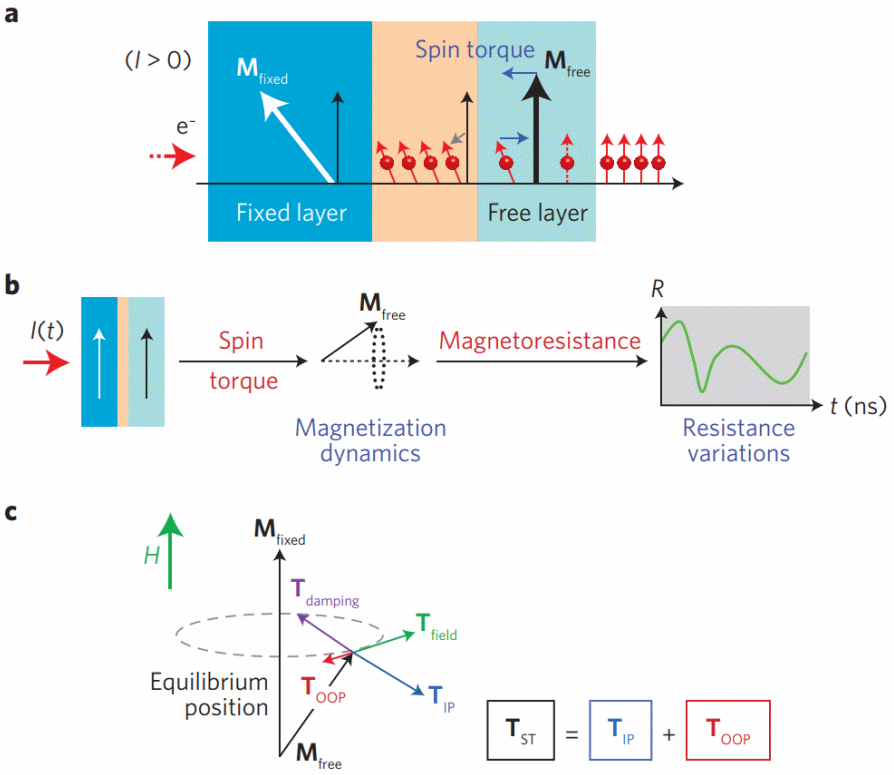

FIGURE 2.6: Schematics of (a) spin-torque effect in a trilayer; (b) magnetization dynamics on nanodevices; (c) torques on the local magnetization, under current infection (credits: [32] N. Locatelli, *et al.*, 2014).

In the case of vortices, a device with non-uniform magnetization, this effect will cause a steady precession in the free layer, resulting in variations of the MTJ's resistance (figure 2.6(b)).

2.5 Neuromorphic spintronics

Spintronic devices are being studied for many interesting applications, one of them being neuromorphic computing. Taking inspiration from the structure of the brain, we can mimic it with MTJ nano-oscillators (making use of their similar stochastic behaviour) to help in many AI algorithms. For instance, Danijela Marković, *et al.* [18] give the example of using spintronic nano-oscillators to recognize spoken words, where we give the corresponding RF wave as the input, and the output is a linear combination of the voltages V_i emitted by the nano-oscillator with weights W_i at different time steps; however, with a lot of noise when we talk about reservoir computing (non-linear type, capable of storing information).

This is possible since we can use this devices to perform analog multiplication, a key operation in convolutional neural networks [33]. This is shown by the Leaky Integrate and Fire (LIF) equation:

$$C\frac{dV}{dt} = -\frac{V}{R} + \sum_j w_j I_j, \tag{2.6}$$

which is used to model neuron behaviour through neuron spikes, where C is the capacitance of the neuron, V the voltage in the membrane, R the resistance of the neuron, w the synaptic weight and I the input current. This behaviour can be copied by magnetic nano oscillator devices, that follow the Landau–Lifshitz–Gilbert–Slonczewski (LLGS) equation (figure 2.6):

$$\frac{d\mathbf{M}}{dt} = -\gamma\mu_0(\mathbf{M}\times\mathbf{H}_{eff}) + \frac{\alpha}{M_s}(\mathbf{M}\times\frac{d\mathbf{M}}{dt}) - \frac{1}{qN_sM_s}(\mathbf{M}\times(\mathbf{M}\times\mathbf{I}_s)) - \frac{\beta}{qN_s}(\mathbf{M}\times\mathbf{I}_s), \tag{2.7}$$

where $\mathbf{M}$ is the magnetization, $\mathbf{H}_{eff}$ is the effective field, $\mathbf{I}_s$ is the applied spin current, γ is the electron gyromagnetic ratio, α is the Gilbert damping constant, β is the field-like torque factor, μ_0 the permeability of free space, M_s is the saturation magnetization, q is the electron charge and N_s is the number of spins, given by $N_s = \frac{2M_s\Omega}{\gamma\hbar}$, where Ω is the volume of the nanomagnet and $\hbar$ is the reduced Planck's constant.

Vortex-based spin torque nano-oscillators have inherent stochasticity and can work as binary non-volatile artifcial synapses [34] and neurons, enabling artificial neural networks (ANN) containing these MTJs to learn.

They can have applications (i) in pattern recognition, (ii) in radar applications where we use spin-based nanodevices as neuron (RF source) and synapse (RF detector), or (iii) in medicine, such as in RF mammography by using nanosynapses, based on MTJs, that directly process the RF signals. Our MTJs will work as the stochastic sigmoid function, to chose if the neuron will fire, when we send input spikes through them to perform a weighted summation.

Chapter 3

Experimental Techniques

In this chapter, we shall go over the methodology used. We're going to examine how the magnetic tunnel junctions were fabricated at INL, analyse the system we're using to characterize the junctions at IFIMUP and explain how that setup is going to give us the information we need about the device in question.

3.1 Fabrication of the MTJs

This work is based on circular micro and nanopillars with several layers, separated in the middle by an insulating crystalline MgO layer. These nanopillars were fabricated at INL [8, 9] and whose main points we are going to detail.

3.1.1 Sputtering

We begin with a sputtering deposition of the MTJ stack with very carefully measured layers of different materials. The sputtering technique (figure 3.1) is a top-down method of physical vapor deposition, where a direct current (DC), in the case of metals or semiconductors, or radio-frequency (RF), in the case of insulators and ferromagnetic metals, potential difference is applied in a given region, causing a bulk material to be hit with charged ions, breaking appart and being sent to a wafer. The choice of materials we decide to use can vary. For instance, in order to accomplish one of the goals of this thesis, we're going to study and compare $NiFe$ and $CoFeSiB$.

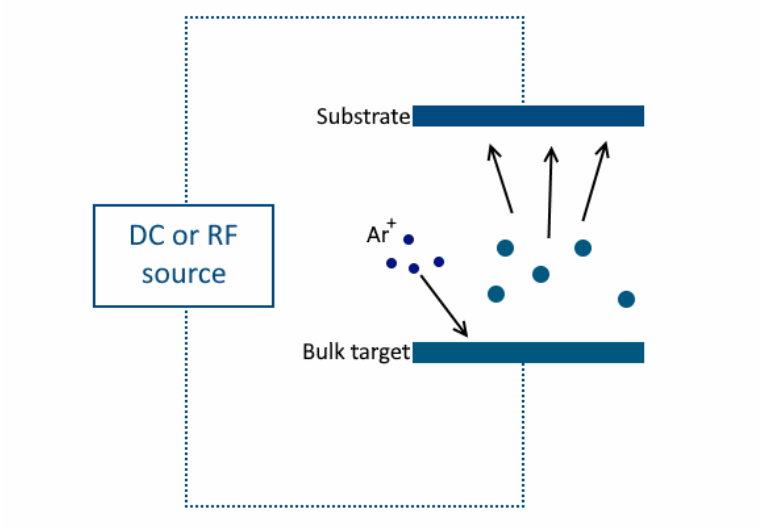

FIGURE 3.1: Schematic of the sputtering principle, where we're using an argon inert gas to create a plasma to hit and break appart the target. These particles will then be deposited in the substrate. The power source can apply a DC or an RF signal.

3.1.2 Lithography

After the deposition, we then use lithography, a method that refers to the use of UV light to create micro and nanoscale patterns who are then washed away. With this technique, we're able to create many diverse types of nanometric structures, including MTJs and much more.

The process starts with the coating of the wafer with photoresist, a polymer that can change its properties when exposed to light. After this, a mask with the desired pattern is placed on top and UV light is used so that only parts of the photoresist change its chemical properties. To create the pillars, however, we use more careful lithography techniques, such as e-beam lithography (for nanopillars) or direct writing (for micropillars).

With this, the wafer can go through a development process, where only the parts of the resist who were exposed to the radiation will be washed away in the process. An etching process, such as ion milling, is then used to remove the parts we do not want in the substract, leaving only the samples and connections we desire to study, and finally, the remaining photoresist can be stripped away. A visual aid of this process can be seen in figure 3.2.

3.1.3 Ion Milling

For the etching process, ion milling was used. This is a physical dry etching process where, just like in the sputtering technique, a beam of ions is accelerated into a sample,

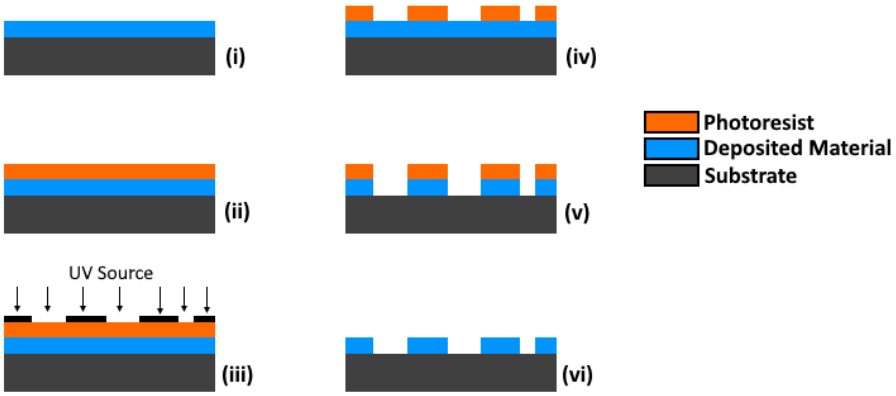

FIGURE 3.2: A scheme of the nanolithography process. Here we see (i) the sample after the sputtering deposition and (ii) with a layer of photoresist, which is then (iii) placed with a mask on top and illuminated with an UV source. The (iv) exposed photoresist is then washed away, which allows (v) the now exposed parts of the deposited material to be removed and then (vi) the remaining photoresist to do the same.

removing atoms from its surface. But unlike sputtering, our goal is just to remove material and not doing deposition; however, some of the removed material might still get redeposited.

This can be a big problem for the pillars, since it causes the MTJ to have a bigger area on its bottom part, leading to undesirable electric and magnetic properties. To solve this, ion milling can also be performed rotating at a sharp angle, for instance, of 170° (where 0° corresponds to the wafer pointing up), so that the removed material can simply fall due to gravity.

3.1.4 Remaining Fabrication Steps

After depositing the MTJ stack through sputtering, doing the lithography process and etching with ion milling, several other combinations of lithographies and etchings are performed so that all the electrical contacts are established. Subsequently, we have an alumina deposition followed by its planarization, where ion milling technique is once again used at an angle for us to achieve a smoother surface.

Finally, after finishing the clean room fabrication, the tunnel junctions go through an annealing procedure to crystallize the various layers and establish an easy axis.

3.2 Characterization of the MTJs

In this section, we'll see the equipment and methods we have available. Starting with our experimental setup (figure 3.3), we're using two Helmholtz coils to generate the magnetic field, which is controled by a signal generator and a power supply [35]. Its actual value is also confirmed by a gaussmeter. To measure the effects on the sample, two probes are connected to its pads. With the help of a sourcemeter, we can then create a current (potential difference) and measure the resulting voltage drop (current).

To control this system, we used labview to connect to our gaussmeter, source meter and signal generator, allowing us to manage the applied values in an easy to manage interface.

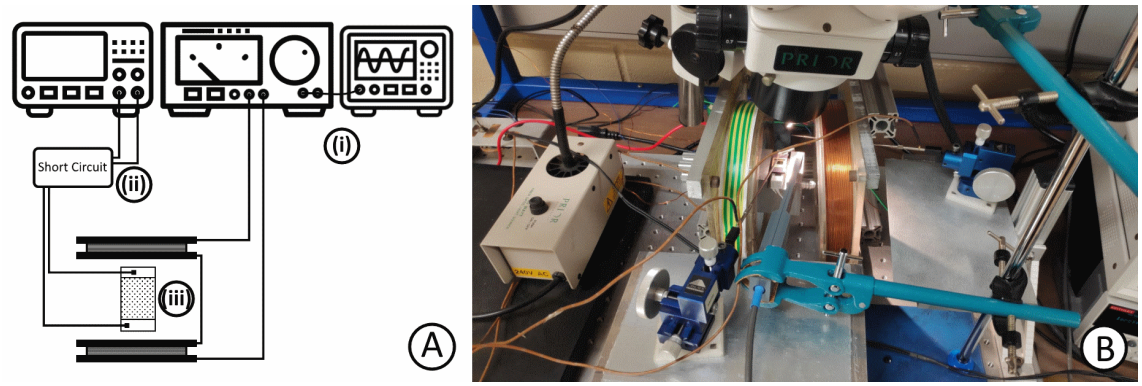

FIGURE 3.3: (a) Schematic of the setup, showing the (i) signal generator and power supply, (ii) source meter (with a device that lets us create a short circuit if needed) and the (iii) sample and coils. (b) Photo of the same setup.

3.2.1 Magnetoresistance

To measure the magnetoresistance, the labview program allows us to choose the values of H_{max}, ΔH, I and $V_{compliance}$. This makes it so that the system varies its applied field from $-H_{max}$ to H_{max} and back in steps of ΔH, applying a current I through the probes and measuring the corresponding voltage drop, never letting the voltage go higher than $V_{compliance}$ (so that the sample doesn't suffer dielectric breakdown).

If we choose so, the software also allows to define an interval $[H_1, H_2]$ where the step changes to ΔH_2 for higher resolution.

3.2.2 Voltage Dependence

In the labview program we can also measure the value of TMR for different voltages and to trace $I-V$ curves. For this, we must input the values of H, V_{max}, ΔV and $I_{compliance}$.

With these values defined, the software makes our instruments vary the voltage between $-V_{max}$ and V_{max} in steps of ΔV, and applies it across the probes, measuring the corresponding current in the process, never letting the current go higher than $I_{compliance}$ (so that the sample doesn't suffer dielectric breakdown). This measurement is made both for an applied external magnetic field of H and $-H$.

More specifically, the labview starts by applying $0V$ and a field of H, measuring the current, then changing it to $-H$ and measuring the current again for that case. After this, the voltage goes to $V = \Delta V$, the same steps are performed, and then again for $V = -\Delta V$. This process continues for $V = 2 \cdot \Delta V$, $V = -2 \cdot \Delta V$, and so on until $V = V_{max}$ and $V = -V_{max}$.

We perform this measurement in this order so that we're increasing and recording the voltage and current slowly around 0, in order to avoid ruining the sample on the first step (for instance, if V_{max} was too high).

With this measurement done, we get two $I-V$ curves (for $+H$ and $-H$) and we may then calculate a $TMR(V)$ curve for each one of this fields by:

$$TMR = \frac{R_{max} - R_{min}}{R_{min}}(\%) = \frac{1/I(H_p) - 1/I(H)}{1/I(H)}(\%), \tag{3.1}$$

in relation to a parallel state given by a field H_p.

3.2.3 Time Oscillations

To explore stochastic behaviour refering to the $I-V$ measurements, we start by choosing values V, H, $I_{compliance}$ and N. During this measurement, the voltage V is held constant and we just change periodically between $+H$ and $-H$, a number of N times, recording the current on each iteration. Once again, we make sure to never let the current go higher than $I_{compliance}$.

We would normally expect that, for each pair V and H, if the same measurement is being done, the resulting graph would be a consistent value. However, if a stochastic behaviour exists, we may see more stable lines, showing the current oscillating with each iteration.

3.2.4 Resistance Density Plot

For this measurement, the software asks for the values of V_{max}, ΔV, H_{max}, ΔH and $I_{compliance}$, working in a similar way to the voltage dependence measurement, explained in section 3.2.2.

Starting at the field $-H_{max}$, we change the voltage (as indicated in section 3.2.2) to obtain an $I-V$ curve for that one specific applied magnetic field. We then increase the value of the field by ΔH and repeat the measurement. We continue this until we reach H_{max}. We record all of these values in a matrix M, where each point corresponds to the current for a given field and voltage.

To analyse a field sweep, we can chose to repeat the measurement, this time, going from $+H_{max}$ to $-H_{max}$.

Since we have the values of V and I for each point, we use Ohm's law to calculate the resistance. Finally, we calculate a new matrix $\tilde{M}$, where each point $\tilde{M}_{ij}$ corresponds to how much the point M_{ij} differs from its neighbours. Therefore, we get a density plot, showing how much the resistance changes from one point to another.

3.2.5 Temperature Dependence

The cryogenics system is composed mainly of a cryostat, a rotary pump, a diffuser pump and a compressor. The cryostat is a device that allows us to achieve temperatures below $123K$ by using certain liquids or gases which will be treated by the compressor. For these cold temperatures to be obtained, pumps are needed to create vacuum, which is important for there not to be heat conduction or convection during the process inside the cryostat, which is protected by two reflective lids, where the outter one is necessary to help protect the environment from the exterior radiation.

To initiallize it, we start by closing the two cryostat lids. After making sure that the secondary valve (and any path to any other cryostat) is closed, we can open the path from the rotary pump and turn on the compressor, with some water running to cool it down. After ~ 10 min, we can close that path and open that of the diffuser pump.

With the system ready, we just need to insert the parameters in the computer. In this case, we will measure magnetoresistance curves, in a similar way to what was explained in section 3.2.1. However, this time we'll examine these parameters for several temperatures, in a range of $25K$ to $300K$.

Chapter 4

Stochastic Behaviour of $NiFe$ MTJ with Vortices

This first study was performed in a micropillar of radius $R = 2.75\ \mu m$ with the composition: 5 Ta / 50 CuN / 5 Ta / 50 CuN / 5 Ta / 5 Ru / 6 $IrMn$ / 2 $CoFe_{30}$ / 0.7 Ru / 2.6 $CoFe_{40}B_{20}$ / MgO 8x193 $3kW$ 600sccm [700 Ohm μm^2] / 2.0 $CoFe_{40}B_{20}$ / 0.21 Ta / 20-42 $NiFe$ wedge (1x pass $14mm/s$ 190% $700W$) / 5 Cu / 10 Ta / 7 Ru (where each number represents the layer's thickness in nanometers).

In the transfer curve present in figure 4.1 we see that the magnetic tunnel junction is giving the expected behaviour discussed previously, changing its magnetization and resistance with the change of the applied magnetic field, saturating at high enough values of H. With the help of equation 3.1, we may obtain the TMR value for each point, obtaining a maximum magnitude of approximately 45%.

Examining the transfer curve more carefully, we may notice several resistance jumps in the region of low magnetic fields. The reason behind this is that, at low H fields, the sample is in the vortex state. Large fields saturate the free layer, but reducing the field, it allows renucleation of the vortex [34]; therefore, at low fields we observe a linear behaviour (as discussed in section 2) with clear jumps in the resistance, which correspond to the vortex traveling through the layer and jumping between different potential minimi created by the grains as the magnetic field moves the vortex core across the pillar.

Having confirmed these properties, our job starts with analysing the tunnel magnetoresistance (TMR) values for different applied magnetic fields H and voltages V. We examine the $I - V$ curves (current as function of voltage) for several applied in-plane

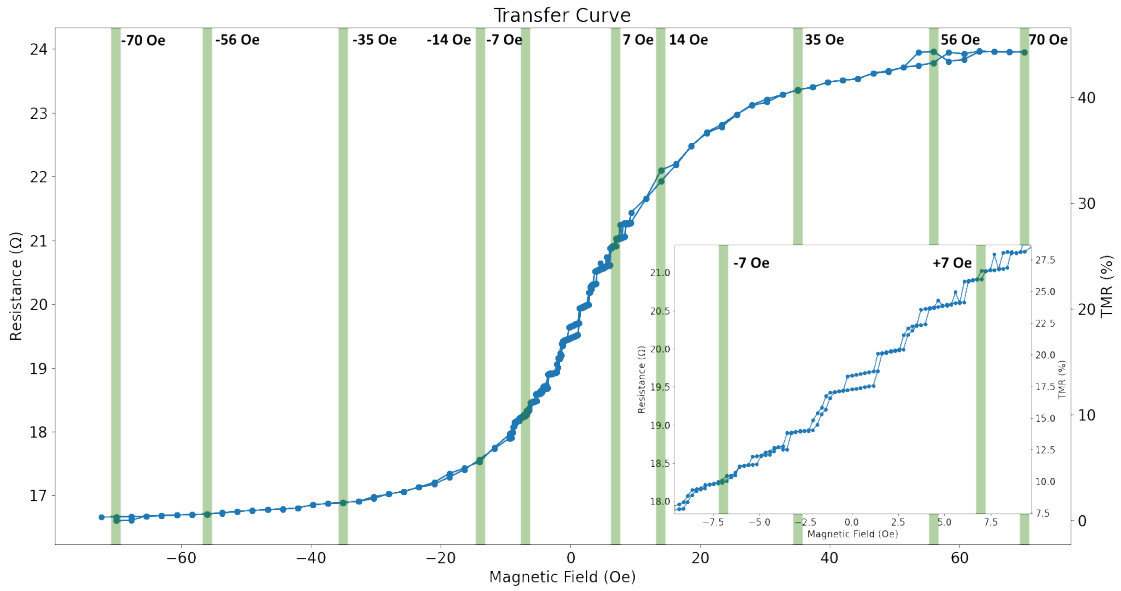

FIGURE 4.1: Transfer curve for the *NiFe* sample, with some of the points we will analyse highlighted in green.

magnetic fields, as we see in figure 4.2, and calculate the TMR(V) curves (figures 4.3 and 4.4) using equation 3.1.

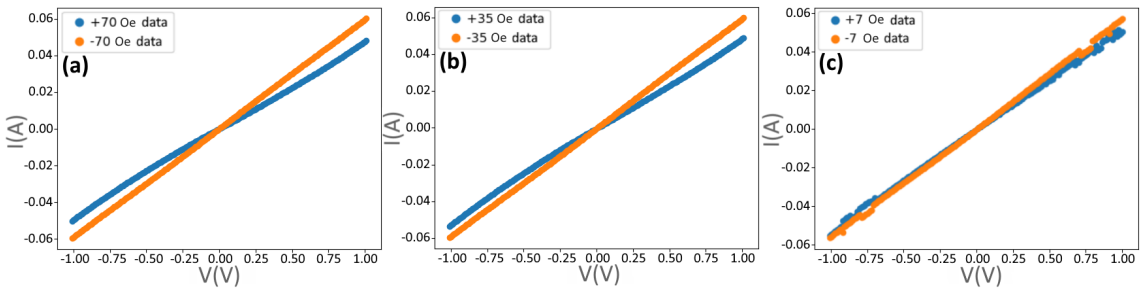

FIGURE 4.2: $I - V$ curves for several applied magnetic fields.

The $I - V$ curves shown in figure 4.2 have an almost linear behaviour; however, we see that, for low magnetic fields and large applied voltages, the current starts to oscillate.

The same oscillating effect can be seen better in the TMR(V) curves. In figure 4.3 we see the behaviour for negative fields. Since -70 Oe corresponds to the minimum resistance and we are using it as a reference, the curve for that value of H is a steady line at 0 (figure 4.3(a)). At $+70$ Oe, as we see in figure 4.4(a), the curve shows a larger TMR when no voltage is applied and decreasing with increasing voltage. For smaller magnetic field

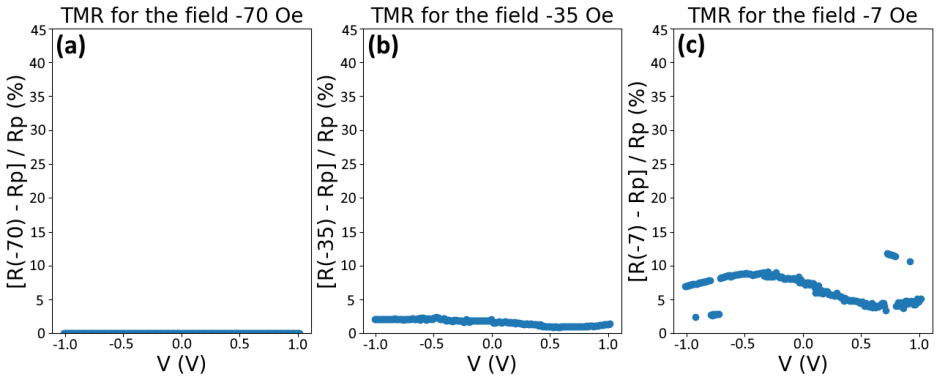

FIGURE 4.3: TMR(V) curves for several applied negative magnetic fields.

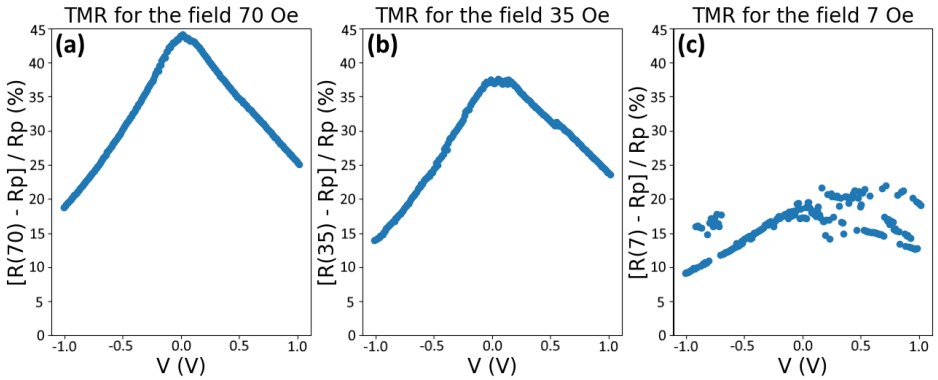

FIGURE 4.4: TMR(V) curves for several applied positive magnetic fields.

magnitudes, in both figures, jumps start to be noticeable in the region of high voltage, which seems to show several "metastable states" that the current may have.

Physically, this means that by applying a small in-plane field and a given voltage, the vortex center will travel through the potential minimi in the free layer and, if the voltage is high enough, it seems that the vortex core is able to jump stochastically into different minimi, originating different values for the resistance; however, a clear physical reason for why this happens is still not clear.

In order to confirm and better study this phenomenon, for different fields, we fixed a voltage and measured the current across a given time frame Δt. We can see the results in figures 4.5 ($H > 0$) and 4.6 ($H < 0$) and we can notice that, for small field values and large voltages, the current value seems to jump into distinct values. This is not seen in samples with no vortices, as we can see by image 4.7, where we conducted the same experiment in a non-vortex-based magnetic tunnel junction and obtain that the current distribution is uniform.

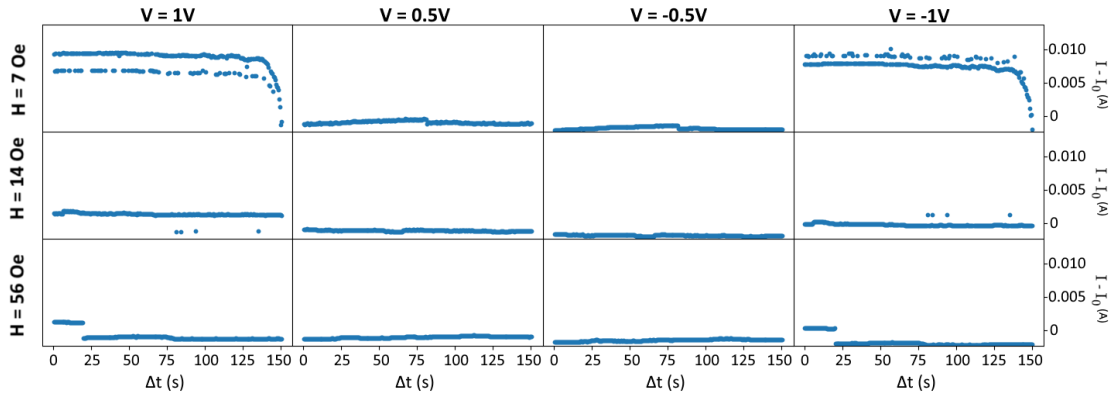

FIGURE 4.5: Current in the vortex-based MTJs at constant V and $H > 0$, where we see clear oscillations at low fields and high voltages (I_0 is an abstract value).

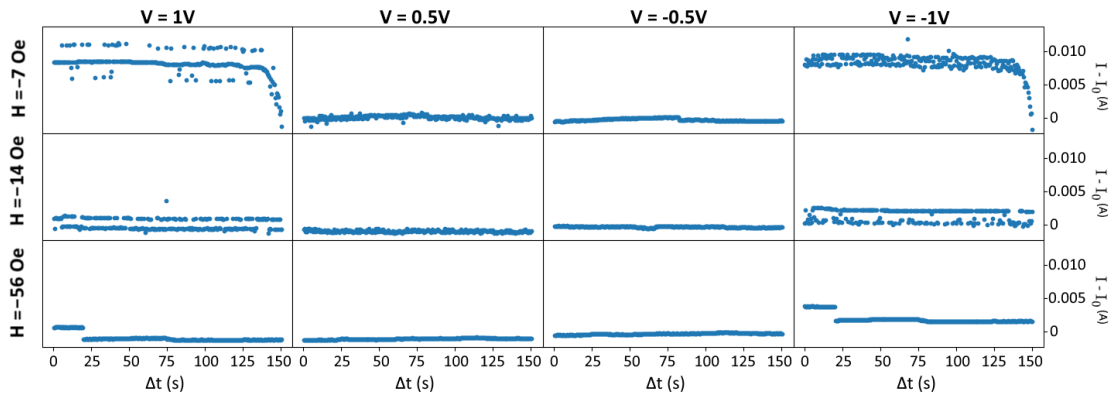

FIGURE 4.6: Current in the vortex-based MTJs at constant V and $H < 0$, where we see clear oscillations at low fields and high voltages (I_0 is an abstract value).

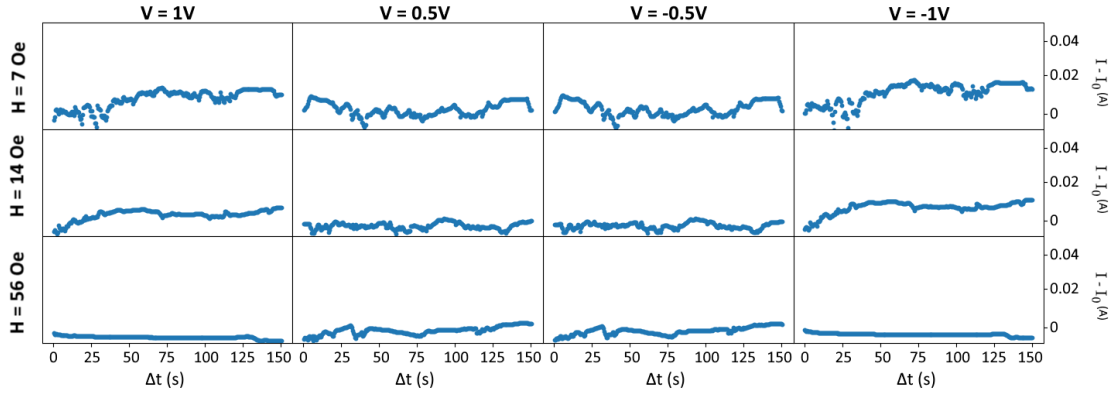

FIGURE 4.7: Current in an MTJ with no vortices at constant V and $H > 0$ (I_0 is an abstract value). Their behaviour for $H < 0$ is equivalent.

Lastly, we sweeped the magnetic field (in steps of $\Delta H = 2.3$ Oe) and the voltage (in steps of $\Delta V = 0.02$ V) in order to make a density plot, as we see in figure 4.8, which shows the change in resistance from on point to another. Once again, we see the biggest variation in the vortex state, with jumps in the resistance that are clearly noticeable, and also a dependence in the applied voltage, with more jumps in higher voltages. Besides that, we also see clearly defined resistance changes when the MTJ starts to leave the vortex state and starts to saturate.

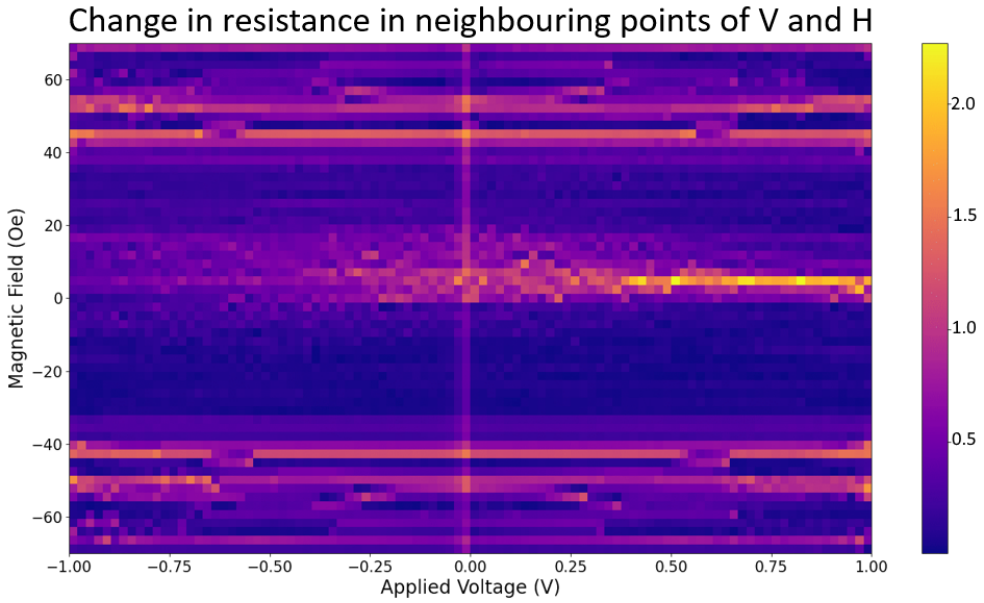

FIGURE 4.8: Variation in resistance dR as a function of the voltage V and the in-plane magnetic field H.

To analyse if there is a dependence in the field sweep direction (from $+H$ to $-H$ or from $-H$ to $+H$), we recreate the previous density plot from -9 to $+9$ Oe, in steps of 0.5 Oe (we need this resolution to see the jumps). We start by going from -9 to $+9Oe$ (exploring the entire voltage range for each H value until $\pm 1V$, in steps of 0.02 V); then, we do the same thing from $+9$ to -9 Oe. The result can be seen in figure 4.9.

Observing the two plots, even though they have some differences, we are not able to conclude that there is any significant disparity on which direction we chose to vary the value of the in-plane magnetic field. Again, the largest resistance variation happens around $H = 0$ for high values of $|V|$. When it comes to the voltage bias dependence, even though we can still notice some higher dR on the high positive side, for this sample, it seems to have a much more symmetrical behaviour, where the biggest variation does happen at high $|V|$, but the difference between $+V$ and $-V$ is not as large as in the previous density plot (figure 4.8).

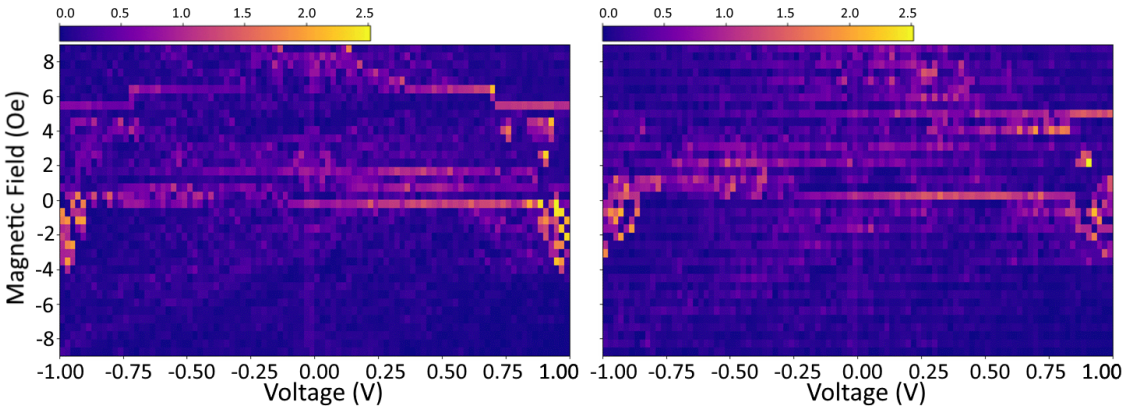

FIGURE 4.9: Variation in resistance dR, in a $NiFe$ sample, as a function of the voltage V and the in-plane magnetic field H, where the left one represents going from $-H$ to $+H$ and the right one from $+H$ to $-H$.

Chapter 5

Magnetoresistance Study of $CoFeSiB$ MTJ with Vortices

This analysis was performed in a nanopillar of radius $R = 150\ nm$ with the composition: 5 Ta / 50 CuN / 5 Ta / 50 CuN / 5 Ta / 5 Ru / 6 $IrMn$ / 2 $CoFe_{30}$ / 0.825 Ru / 2.6 $CoFe_{40}B_{20}$ / MgO [8 Ohm μm^2] / 2.0 $CoFe_{40}B_{20}$ / 0.21 Ta / 6-13 $CoFeSiB$ wedge (1x pass $20mm/s$ 200%) / 10 Ta / 7 Ru (where each number represents the layer's thickness in nanometers).

We're now studying a much thinner $CoFeSiB$ sample. This one shows less hysteresis and, by being smaller, a fewer amount of jumps. So, we aim to be able to detect and study them more easily with the same resolution.

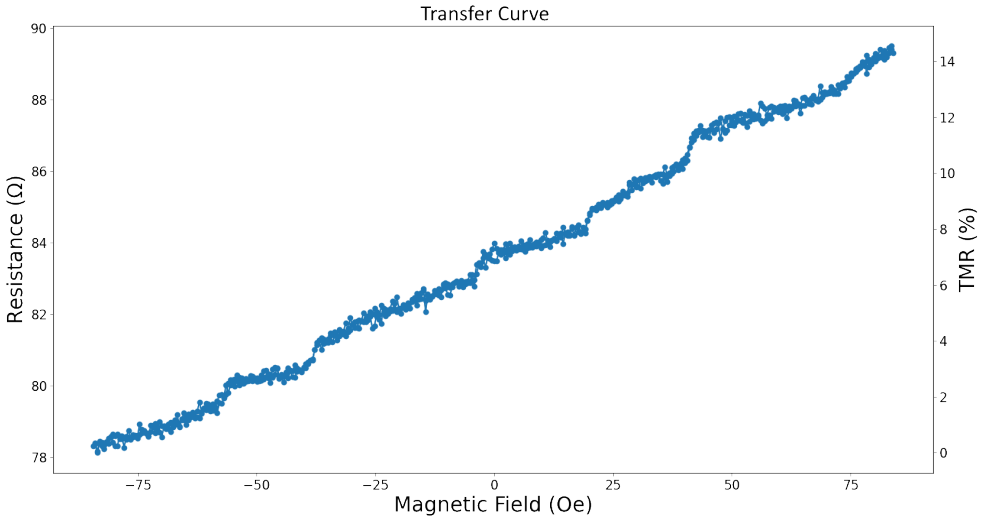

FIGURE 5.1: Transfer curve for the $CoFeSiB$ sample.

Starting once again with the transfer curve, we obtain figure 5.1 and we can see that the jumps are clearly noticeable and that the vortex state persists across the entire magnetic field range we're applying, never saturating, and reaching a TMR magnitude of 14%.

After obtaining the transfer curve, the first thing we decided to do was to study the sample's behaviour with changing voltage, just like we did with the $NiFe$ sample. Since this sample stays in the vortex state even for large fields, we can also use them in order to determine the MTJ's vortex properties. However, this smaller wedge doesn't stand the high voltage values we applied previously, so we'll limit the bias to only $0.24V$, resulting in a linear $I - V$ relation, for any applied field. Combining our results into density plots showing the change in resistance, we obtain figure 5.2, where, once again, steps of $\Delta H =$ 0.5 Oe and $\Delta V = 0.02$ V were used.

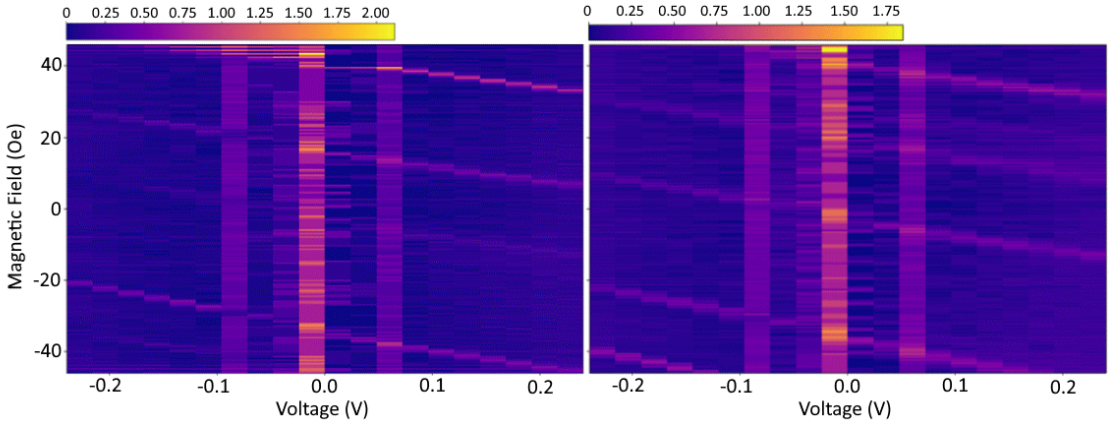

FIGURE 5.2: Variation in resistance dR, in a $CoFeSiB$ sample, as a function of the voltage V and the in-plane magnetic field H, where the left one represents going from $-H$ to $+H$ and the right one from $+H$ to $-H$.

First of all, by looking at the two plots, there doesn't seem to be a difference between the $MR(H)$ sweeping directions. However, when it comes to its voltage bias dependence, we see that, once again, it has a clear effect on the vortex core jumps. The highest jumps seem concentrated around $V = 0$ and increasing the voltage leads them to be smaller. We can also notice that a variation in the applied bias causes the jumps to slightly shift their location. This can be seen better in figure 5.3(a), where we notice that positive voltages cause the jumps to happen sooner (needing a lower magnetic field) and negative voltages cause them to happen later (needing a higher magnetic field) in what seems like a linear variation.

Having then obtained clearly defined jumps for this sample, our last task involved

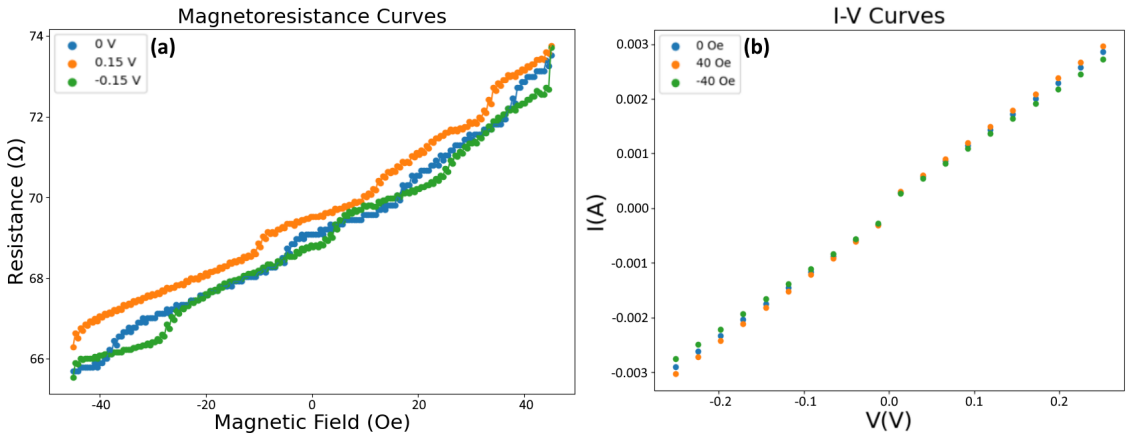

FIGURE 5.3: (a) Magnetoresistance curves for 3 voltage bias and (b) $I - V$ curves for 3 applied magnetic fields for the *CoFeSiB* sample.

studying how they change with temperature. With the help of a cryostat capable of reaching 25K, as detailed in section 3.2.5, we obtained the transfer curves for several temperatures, as depicted in figure 5.4.

At 300K (room temperature), figure 5.4 shows a transfer curve very similar to that of figure 5.1 and, at lower temperatures, we can see a slight increase of the TMR value, as the literature says it tends to happen. Regarding the jumps, the graphs show that, as temperature lowers, these become sharper and some hysteresis starts to appear, as we see more clearly from figure 5.5, which shows the derivative of the transfer curves.

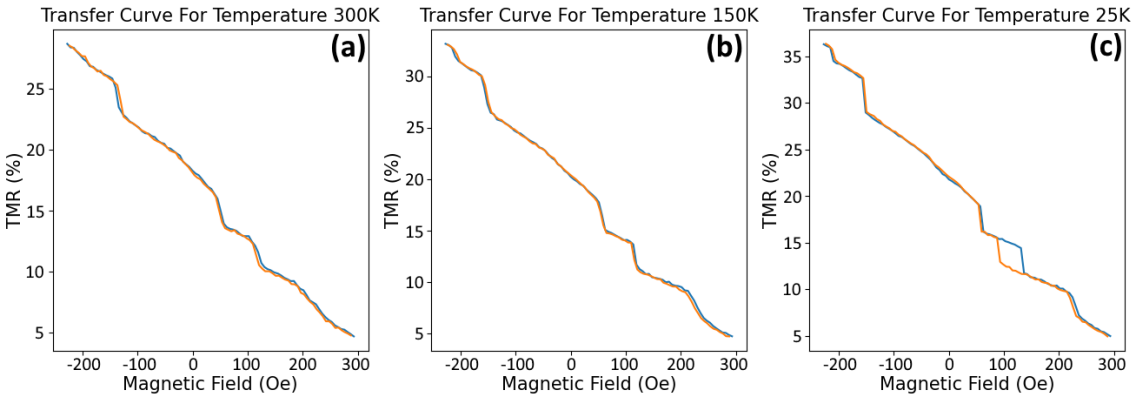

FIGURE 5.4: Transfer curves for a sample with *CoFeSiB* wedge at different temperatures, where the blue curve represents going from $-H$ to $+H$ and the orange curve from $+H$ to $-H$.

For the 5 main jumps that we are able to see in the transfer curve, as figure 5.6(a) indicates, we see in figure 5.6(b) that hysteresis becomes more prominent as temperature decreases (specially with jump number 4). We believe this is due to the fact that, during a jump at room temperature, the vortex core has thermally assisted switching between the

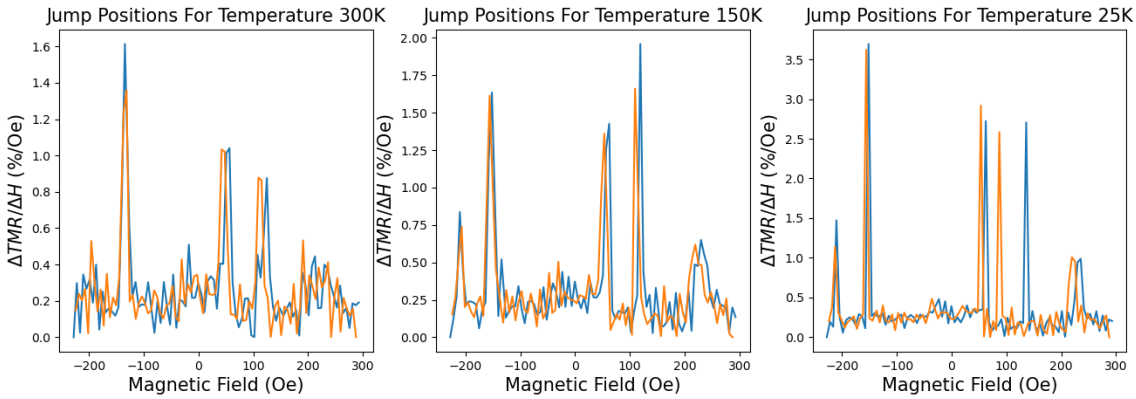

FIGURE 5.5: The derivative of the TMR with the field, in which we see the positions of the sharp jumps for the transfer curves for a sample with $CoFeSiB$ wedge at different temperatures, where the blue curve represents going from $-H$ to $+H$ and the orange curve from $+H$ to $-H$.

two minimi, fluctuating between them, resulting in a resistance which is a time averaged value of this switching, causing a smooth transition between the two resistance values, as seen in figure 5.7, where we start with the system only spending 29% of the time in the highest resistance (figure 5.7(a)) and then it increases to 49% (figure 5.7(b)) and 78% (figure 5.7(c)). At lower temperatures, however, this switching effect is not present.

On the other hand, we also notice that the position of the jumps is kept stable as we change temperature. This can be seen in figure 5.6(e), where it's represented the mean field of each jump, but also in figures 5.6(c) and 5.6(d), which show the start and end points of the jumps, respectively. However, these two values vary very slightly, leading to figure 5.6(f), which shows a general decrease of the range of each jump as temperature lowers, except when hysteresis starts to take over (as we see in jump number 4), increasing the jump range. This emerges from the lack of thermal energy, causing the jumps to happen later and, in the case of jump number 4, hysteresis to appear.

In figure 5.6(g), it is represented the ΔH interval between each jump. According to equation 2.5, which says that $E_{pin} \propto \Delta H^2$, the energy of the pinning sites would then be proportional to the square of the values present in figure 5.6(g). They would have the values around 1.47 eV (for interval $1-2$), 0.80 eV (for interval $2-3$), 0.57 eV (for interval $3-4$) and 1.81 eV (for interval $4-5$). Through the figure, we notice that the energy of the pinning sites maintains a steady value across temperature. This is not the expected behaviour, as we would expect that lower temperatures would lead to an increase in the depinning energy, needing an higher field to move the vortex core [36, 37].

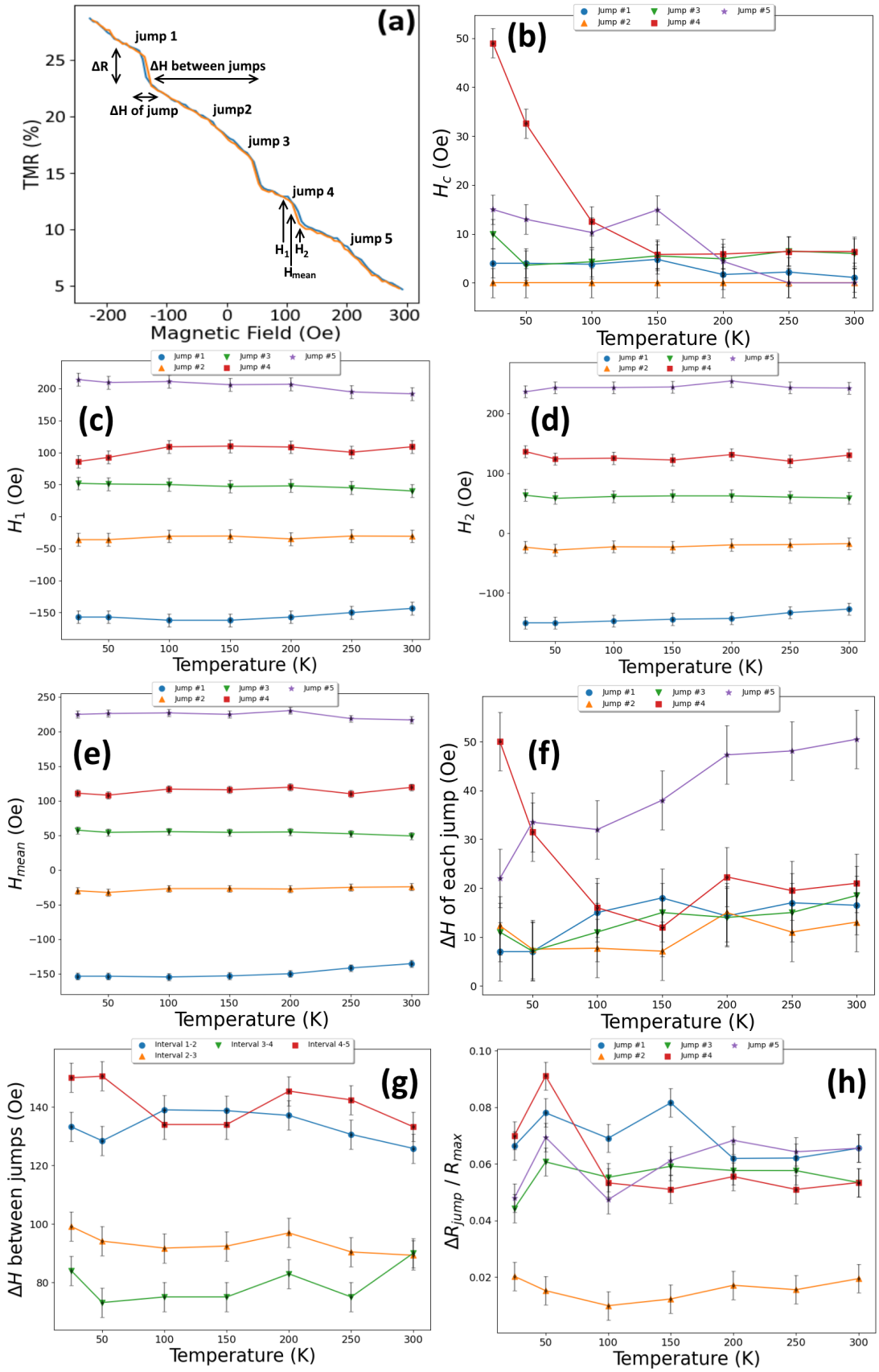

FIGURE 5.6: For the 5 jumps in the (a) transfer curve, it is shown the (b) variation of the field H_c, the (c) starting, (d) final and (e) mean field of each jump, the (f) ΔH duration of each jump, the (g) ΔH interval between jumps (h) resistance drop ΔR of each jump divided by the maximum resistance.

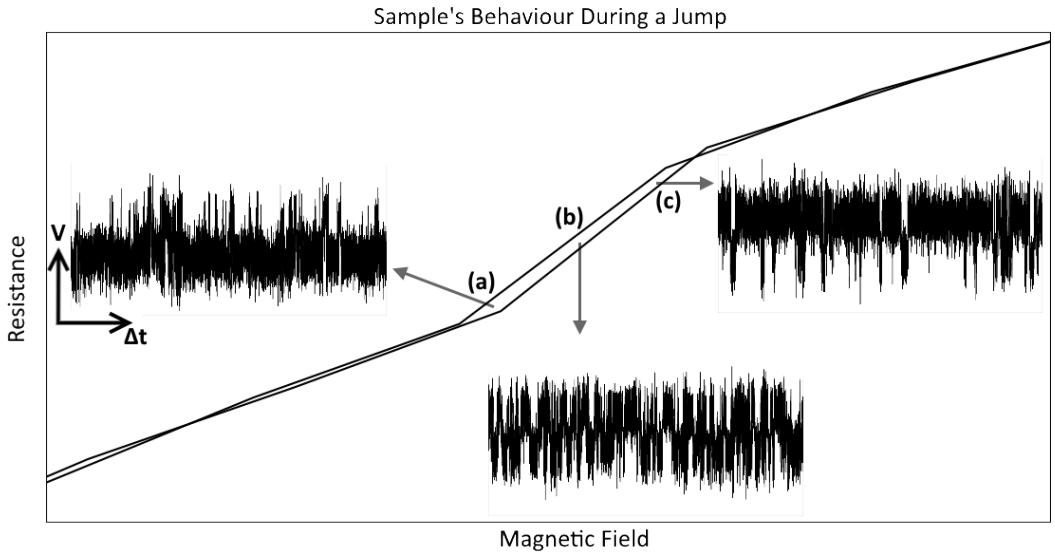

FIGURE 5.7: Resistance jump on a sample with $CoFeSiB$ wedge, with the corresponding oscilloscope resistance variation measurement at the (a) lowest, (b) middle and (c) highest points of the jump.

Finally, in figure 5.6(h) we represent the change in resistance of each jump divided by its maximum resistance at each temperature T, which we already saw it tends to increase with temperature (figure 5.4). The result is independent of T, what can lead to the conclusion that any change in ΔR that may be seen in the jumps is only consequence of the total change in resistance.

Chapter 6

Conclusions

In the MTJs that we studied, we were able to see stochastic current behaviour at low fields, when the system is in its vortex state. This behaviour corresponds to the vortex core stochastically switching between pinning sites, resulting in different resistance values; however, this behaviour is only observed if high voltages are applied. On thinner samples, where jumps are more defined, voltage bias was also observed to be able to lag or aid the position of said jumps.

Due to this stochastic behaviour at low magnetic fields due to granularity induced vortices, we may conclude that we can use this micromagnetic structures for neuromorphic applications. These stochastic bits may be useful for random number generators, for combinatorial optimization, probabilistic inference or random walks, making them useful for artificial neural networks.

Finally, a temperature dependence was studied, where we saw that lower temperatures cause the appearance of hysteresis and sharper jumps due to the lack of thermally assisted switching between pinning sites. However, we were not able to observe a change in the pinning energy as a function of temperature.

In future works, these dependences can be studied and better understood, such as the voltage bias dependence that was observed, for which a reason for its behaviour is still not clear. Besides that, a better analysis of how temperature affects these devices can and should be performed, namely studying $I - V$ curves at low temperatures or even connecting the oscilloscope to the cryostat to see how the sample's behaviour during a jump changes in cryogenic conditions. Both these experiments could give useful information to get a better grasp of the inner workings of magnetic tunnel junctions, which could be fruitful in future applications.

Bibliography

[1] J. M. D. Coey, *Magnetism and Magnetic Materials*. Cambridge University Press, 2009. [Cited on pages 1 and 3.]

[2] S. H. Simon, *The Oxford Solid State Basics*. Oxford University Press, 2013. [Cited on pages 1 and 9.]

[3] U. Jeong, X. Teng, Y. Wang, H. Yang, and Y. Xia, "Superparamagnetic colloids: Controlled synthesis and niche applications." *Advanced Materials*, 2007. [Cited on pages xi and 2.]

[4] D. Kirk, A. Kohn, K. Borisenko, C. Lang, J. Schmalhorst, G. Reiss, and D. COCKAYNE, "Structural study of amorphous CoFeB thin films exhibiting in-plane uniaxial magnetic anisotropy," *PHYSICAL REVIEW B*, 2009. [Cited on pages xi and 3.]

[5] T. Shinjo, *Nanomagnetism and Spintronics*. Elsevier, 2009. [Cited on page 3.]

[6] M. Ziese and M. J. Thornton, *Spin Electronics*. Springer, 2001. [Cited on page 3.]

[7] S. M. Thompson, "Topical review: The discovery, development and future of gmr: The nobel prize 2007," *J. Phys. D: Appl. Phys.*, 2008. [Cited on pages xi and 4.]

[8] L. J. F. Martins, "CoFeB/MgO/CoFeB-based magnetic tunnel junctions for memory applications: optimization of the fabrication process and magnetic properties," Master's Thesis, Faculty of Sciences of the University of Porto, 2016. [Cited on pages 4, 9, 10, and 17.]

[9] J. M. M. Teixeira, "MgO-based magnetic tunnel junctions: Physical studies," Master's Thesis, Faculty of Sciences of the University of Porto, 2010. [Cited on pages 4, 10, and 17.]

[10] J. gang Zhu and C. Park, "Magnetic tunnel junctions," *Materials Today*, 2006. [Cited on page 5.]

[11] I. Žutić, J. Fabian, and S. D. Sarma, "Spintronics: Fundamentals and applications," *Rev. Mod. Phys.*, 2004. [Cited on pages xi and 5.]

[12] M. Julliere, "Tunneling between ferromagnetic films," *Physics Letters A*, 1975. [Cited on page 5.]

[13] I. A. Campbell, A. Fert, and R. Pomeroy, "Evidence for two current conduction iron," *The Philosophical Magazine: A Journal of Theoretical Experimental and Applied Physics*, 1967. [Cited on pages 5 and 6.]

[14] A. Fert and I. A. Campbell, "Two-current conduction in nickel," *Phys. Rev. Lett.*, 1968. [Cited on page 5.]

[15] A. Kent and D. Worledge, "A new spin on magnetic memories," *Nature Nanotechnology*, 2015. [Cited on page 6.]

[16] P. M. Tedrow and R. Meservey, "Spin-dependent tunneling into ferromagnetic nickel," *Phys. Rev. Lett.*, 1971. [Cited on page 6.]

[17] A. Houshang, E. Iacocca, P. Dürrenfeld, S. R. Sani, J. Åkerman, and R. K. Dumas, "Spin-wave-beam driven synchronization of nanocontact spin-torque oscillators," *Nature Nanotechnology*, 2016. [Cited on page 6.]

[18] D. Marković, A. Mizrahi, and J. G. D Querlioz, "Physics for neuromorphic computing," *Nature Reviews Physics*, 2020. [Cited on pages 7 and 15.]

[19] S. Yuasa and D. D. Djayaprawira, "Giant tunnel magnetoresistance in magnetic tunnel junctions with a crystalline MgO(0 0 1) barrier," *Journal of Physics D: Applied Physics*, 2007. [Cited on pages xi and 10.]

[20] Y. Nagamine, H. Maehara, K. Tsunekawa, D. Djayaprawira, N. Watanabe, S. Yuasa, and K. Ando, "Ultralow resistance-area product of 0.4 $\Omega(\mu m)^2$ and high magnetoresistance above 50% in CoFeB/MgO/CoFeB magnetic tunnel junctions," *Applied Physics Letters*, 2006. [Cited on page 9.]

[21] E. Tsymbal, O. Mryasov, and P. Leclair, "Spin-dependent tunnelling in magnetic tunnel junctions," *Journal of Physics: Condensed Matter*, 2003. [Cited on pages xi and 11.]

[22] S. Zhang, P. M. Levy, A. C. Marley, and S. S. P. Parkin, "Quenching of magnetoresistance by hot electrons in magnetic tunnel junctions," *Phys. Rev. Lett.*, 1997. [Cited on page 10.]

[23] M. Sharma, S. X. Wang, and J. H. Nickel, "Inversion of spin polarization and tunneling magnetoresistance in spin-dependent tunneling junctions," *Physical Review Letters*, 1999. [Cited on page 10.]

[24] C. H. Shang, J. Nowak, R. Jansen, and J. S. Moodera, "Temperature dependence of magnetoresistance and surface magnetization in ferromagnetic tunnel junctions," *Phys. Rev. B*, 1998. [Cited on page 11.]

[25] H. X. Wei, Q. H. Qin, M. Ma, R. Sharif, and X. F. Han, "80% tunneling magnetoresistance at room temperature for thin al–o barrier magnetic tunnel junction with cofeb as free and reference layers," *Journal of Applied Physics*, 2007. [Cited on pages xi and 11.]

[26] K. L. Metlov and K. Y. Guslienko, "Stability of magnetic vortex in soft magnetic nano-sized circular cylinder," *Journal of Magnetism and Magnetic Materials*, 2002. [Cited on page 12.]

[27] K. Y. Guslienko, V. Novosad, Y. Otani, H. Shima, and K. Fukamichi, "Field evolution of magnetic vortex state in ferromagnetic disks," *Applied Physics Letters*, 2001. [Cited on pages xi and 12.]

[28] S. Wittrock, P. Talatchian, M. Romera, M. J. Garcia, M.-C. Cyrille, R. Ferreira, R. Lebrun, P. Bortolotti, U. Ebels, J. Grollier, and V. Cros, "Flicker and random telegraph noise between gyrotropic and dynamic c-state of a vortex based spin torque nano oscillator," *AIP Advances*, 2021. [Cited on page 13.]

[29] S. Wittrock, P. Talatchian, M. Romera, S. Menshawy, M. J. Garcia, M.-C. Cyrille, R. Ferreira, R. Lebrun, P. Bortolotti, U. Ebels, J. Grollier, and V. Cros, "Beyond the gyrotropic motion: Dynamic c-state in vortex spin torque oscillators," *Applied Physics Letters*, 2021. [Cited on page 13.]

[30] M. J. Garcia, J. Moulin, S. Wittrock, S. Tsunegi, K. Yakushiji, A. Fukushima, H. Kubota, S. Yuasa, U. Ebels, M.Pannetier-Lecoeur, C. Fermon, R. Lebrun, P. Bortolotti, A. Solignac, and V. Cros, "Spin-torque dynamics for noise reduction in vortex-based sensors," *Appl. Phys. Lett.*, 2021. [Cited on page 13.]

[31] C. TY, E. MJ, C. PA, and L. C., "Surface roughness dominated pinning mechanism of magnetic vortices in soft ferromagnetic films," *Physical Review Letters*, 2012. [Cited on page 13.]

[32] N. Locatelli, V. Cros, and J. Grollier, "Spin-torque building blocks," *Nature Materials*, 2014. [Cited on pages xi and 14.]

[33] L. Mazza, V. Puliafito, E. Raimondo, A. Giordano, Z. Zeng, M. Carpentieri, and G. Finocchio, "Computing with injection-locked spintronic diodes," *Phys. Rev. Applied*, 2022. [Cited on page 15.]

[34] L. Martins, A. S. Jenkins, L. S. E. Alvarez, J. Borme, T. Böhnert, J. Ventura, P. P. Freitas, and R. Ferreira, "Non-volatile artifcial synapse based on a vortex nano-oscillator," *Scientific Reports*, 2021. [Cited on pages 15 and 23.]

[35] A. Campilho, *Instrumentação Eletrónica. Métodos e Técnicas de Medição*. FEUP Edições, 2000. [Cited on page 20.]

[36] P. Lendecke, R. Eiselt, G. Meier, and U. Merkt, "Temperature dependence of domain-wall depinning fields in constricted permalloy nanowires," *Journal of Applied Physics*, 2008. [Cited on page 32.]

[37] P. Dagras, M. Kläui, M. Laufenberg, D. Bedau, L. Vila, G. Faini, C. A. F. Vaz, J. A. C. Bland, and U. Rüdiger, "The influence of thermal activation and the intrinsic temperature dependence of the spin torque effect in current-induced domain wall motion," *Journal of Physics D: Applied Physics*, 2007. [Cited on page 32.]